Molecularly Rigid Microporous Polyamine Captures and Stabilizes Conducting Platinum Nanoparticle Networks

Daping He [1], Dong Sheng He [2], Jinlong Yang [3], Ze-Xian Low [4], Richard Malpass-Evans [5], Mariolino Carta [5], Neil B. McKeown [5], and Frank Marken*[1]

[1] Department of Chemistry, University of Bath, Claverton Down, Bath BA2 7AY, UK

[2] Materials Characterization and Preparation Center, South University of Science and Technology of China, Shen-Zhen, 518055, China

[3] School of Advanced Materials, Peking University Shenzhen Graduate School, Shenzhen 518055, China

[4] Centre for Advanced Separations Engineering, Department of Chemical Engineering, University of Bath, Claverton Down, Bath BA2 7AY, UK

[5] School of Chemistry, University of Edinburgh, David Brewster Road, Edinburgh, EH9 3FJ, UK

KEYWORDS: tunneling; electrocatalysis; fuel cells; membrane; stabilization; percolation.

ABSTRACT: A molecularly rigid polyamine based on a polymer of intrinsic microporosity (PIM-EA-TB) is shown to capture and stabilize platinum nanoparticles during colloid synthesis in the rigid framework. Stabilization here refers to avoiding aggregation without loss of surface reactivity. In the resulting rigid framework with embedded platinum nanoparticles, the volume ratio of platinum to PIM-EA-TB in starting materials is varied systematically from approximately 1.0 to 0.1 with the resulting platinum nanoparticle diameter varying from approximately 4.2 to 3.1 nm, respectively. Elemental analysis suggests that only a fraction of the polymer is "captured" to give nano-composites rich in platinum. A transition occurs from electrically conducting and electrochemically active (with shorter average inter-particle distance) to a non-conducting only partially electrochemically active (with longer average inter-particle distance) polymer - platinum composites. The conducting nanoparticle network in the porous rigid macromolecular framework could be beneficial in electrocatalysis and in sensing applications.

Introduction. The formation of platinum (Pt) colloids in aqueous or organic solvent media is based on a complex process with nucleation and growth steps resulting in a diverse range of nano-catalysts.[1] Without suitable capping or stabilization agents, growth processes and Ostwald ripening can dominate to give bigger less well-defined particles.[2] Many stabilization agents have been developed and optimized, for example, based on water-soluble polymers such as poly-(N-vinyl-2-pyrrolidone) (PVP[3,4]) or nanoparticles have been grown into solid microporous hosts such as metal-organic frameworks.[5] These polymer or microporous agents provide conditions for uniform growth, shape control, and confinement effects to prevent aggregation of nanoparticles. However, the strong organic "shell" coated onto the Pt nanoparticle surface can be detrimental and hard to remove, which reduces the availability of active surface sites and hampers application in areas such as efficient catalysis. The development of new protecting/stabilizing agents to increase the Pt utilization is thus desired. New molecularly rigid "framework" polymer molecules could play an important role in providing stabilization without coating the platinum surface.

Polymers of intrinsic microporosity[6,7] (PIMs) have emerged as a novel class of molecular structures with applications (and the corresponding theory) emerging in gas separation and sorption.[8,9] In recent years molecularly rigid polyamine systems such as PIM-EA-TB[10] have been developed with unusual properties such as high surface area (Brunauer–Emmett–Teller or BET surface area of 1027 m^2g^{-1}), rigid pores of typically 1-2 nm diameter, and excellent processibility. Application have been suggested as active component for optical gas sensors,[11] as ionic diodes in electrolyte media,[12,13] and desalination processes.[14] Applications in electrocatalysis have been suggested for the "*in situ*" stabilization of nanoparticle catalysts in fuel cells,[15,16] and as a framework for molecular electrocatalysts such as FeTPP[17] and TEMPO.[18] Recent publications have demonstrated that microporous PIM-EA-TB can be employed in both acidic and alkaline aqueous electrolyte media.

Previous studies on composites with PIM "framework" have been reported on graphene – PIM-1[19] and on palladium "infusion" into a microporous polymer.[20] Catalysis reactions were investigated for platinum nanoparticles in a hyper-crosslinked

polystyrene composite.[21] Here, the stabilizing effects of the molecularly rigid polyamine PIM-EA-TB on the platinum nanoparticle nucleation and growth process are investigated. As illustrated in Figure 1, the platinum precursor $PtCl_6^{2-}$ is proposed to adsorb into the PIM-EA-TB polymer (similar to the $PdCl_4^{2-}$ absorption reported previously[22]) followed by alkaline reduction with ethylene glycol at 130 °C to give platinum nanoparticles dispersed within the PIM-EA-TB polymer framework at fixed sites. The average distance between platinum nanoparticles can be controlled by the volume ratio of platinum to PIM-EA-TB. This allows novel microporous materials to be obtained with variable conductivity switching from a fully conducting material at short average distance to a poorly conductive material at longer average distance.

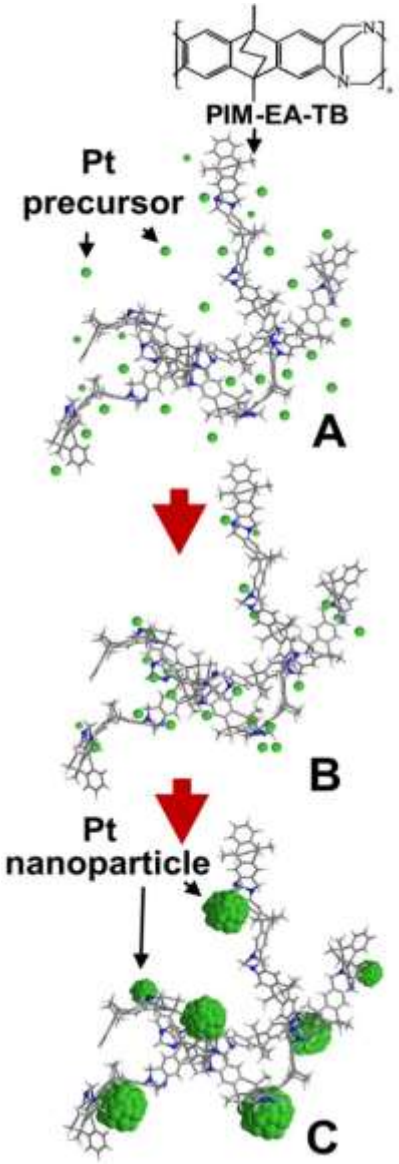

Figure 1. Schematic drawing of (A) Pt precursor diffusion into micropores, (B) adsorption to N-sites, and (C) the nucleation and growth of platinum nanoparticles in the presence of the rigid PIM-EA-TB capture agent (see molecular structure).

Experimental

Chemical reagents. $H_2PtCl_6 \cdot H_2O$ (39.89 wt. % Pt) was purchased from Johnson–Matthey. Ethylene glycol (EG), dimethylformamide (DMF), isopropanol, and perchloric acid (70%–72%), were obtained from Sigma-Aldrich and used without further purification. PIM-EA-TB was synthesized following a literature recipe.[10] Solutions were prepared with filtered and deionized water of resistivity 18.2 MΩ cm taken from a Thermo Scientific water purification system.

Instrumentation. Electrochemical measurements were conducted with a potentiostat system (μAutolab III) with a KCl-saturated calomel reference (SCE, Radiometer, Copenhagen) and platinum wire counter in a three-electrode cell. Morphologies of the prepared catalysts were analyzed with a JEOL 2010 high-resolution transmission electron microscope (HRTEM). XRD spectra were obtained on X-ray diffraction (XRD Bruker D8 ADVANCE, Madison, WI, USA) with a mono-chromatized source of Cu-Kα radiation. The chemical composition and valence state was analyzed by X-ray photoelectron spectroscopy (XPS, PHI Quantera, U-P). Elemental microanalysis was performed by Butterworth Laboratories, London, UK.

Procedures for colloid and electrode preparation. The Pt@PIM colloid were synthesized in an alkaline ethylene glycol (EG) solution. A volume of 1 mL $H_2PtCl_6 \cdot H_2O$ solution (1.5 mg mL^{-1} in EG) and 100, 300, 500 or 1000 μL PIM-EA-TB dispersion (1 mg PIM-EA-TB powder ml^{-1} in DMF) were added to 10 mL EG. Next, the pH value of this solution was adjusted to 8–10 (monitored with pH paper) by adding aqueous 0.1 M NaOH solution. The solution was then heated at 130 °C for 2 h, during which the colour changed from yellow to black. Then the mixture was cooled down to room temperature. The products were separated by centrifugation and further purified by washing with ethanol. Finally, samples were dispersed in 5 mL ethanol to give Pt, Pt@1PIM, Pt@3PIM, Pt@5PIM, and Pt@10PIM colloids (see Figure 2a). Pure Pt colloid was prepared in the same way but without addition of PIM-EA-TB. Elemental analysis suggests for Pt@1PIM Pt 97.7 %, C 1.7 %, for Pt@3PIM Pt 96.7 %, C 1.8 %, for Pt@5PIM Pt 94.7 %, C 2.2 %, for Pt@10PIM Pt 91.6 %, C 2.1 %.

Electrodes were prepared by drop casting. After 15 min sonication, a volume of 3 μL of the prepared Pt colloids was loaded onto a 3 mm diameter glassy carbon electrode (GC, BAS UK Ltd.). The catalyst layer was allowed to dry under ambient conditions before performing electrochemical measurements.

Results and Discussion

Formation and characterization of platinum nanoparticle networks in PIM-EA-TB. Figure 2a shows a photograph of the ethanolic suspensions of Pt, Pt@1PIM, Pt@3PIM, Pt@5PIM, and Pt@10PIM after 12 h sedimentation time. The Pt suspended in ethanol without PIM-EA-TB eventually settled after about 1 h. However, the Pt@3PIM colloid and the more PIM-EA-TB rich materials resulted in a black colloidal solution without visible precipitation even after 12 h. This implies that the colloidal solution based on PIM-EA-TB is stable

in ethanol. The XRD pattern for the Pt, Pt@1PIM, Pt@3PIM, Pt@5PIM, and Pt@10PIM are shown in Figure 2b. The peaks between 30° and 90° diffraction angles can be indexed to Pt crystals with a face-centred cubic (fcc) structure. The peaks at 2θ = 39.7, 46.5, 67.7, and 81.4° are assigned to the (1 1 1), (2 0 0), (2 2 0), and (3 1 1) planes of Pt, respectively. It can be seen that in addition to nanoparticles getting smaller with more PIM-EA-TB (leading to peak broadening) also the faceting changes with a new broad peak appearing at ca. 50°. The volume-averaged particle size was estimated according to the Scherrer equation.[23]

$$d = k\,\lambda/\beta\cos\theta \qquad (1)$$

Here constant k = 0.89, λ (the X-ray wavelength for Cu radiation) = 0.1541 nm, β is the peak width at half-height, θ is the Bragg angle corresponding to the peak maximum, and d denotes the average diameter of the nanocrystal pellets. From the full-width half-maximum of the (1 1 1) peak, the average Pt particle sizes are estimated as 6.1, 4.3, 3.2, 3.2, and 3.1 nm for Pt, Pt@1PIM, Pt@3PIM, Pt@5PIM, and Pt@10 PIM, respectively. These values are consistent with TEM data (*vide infra*).

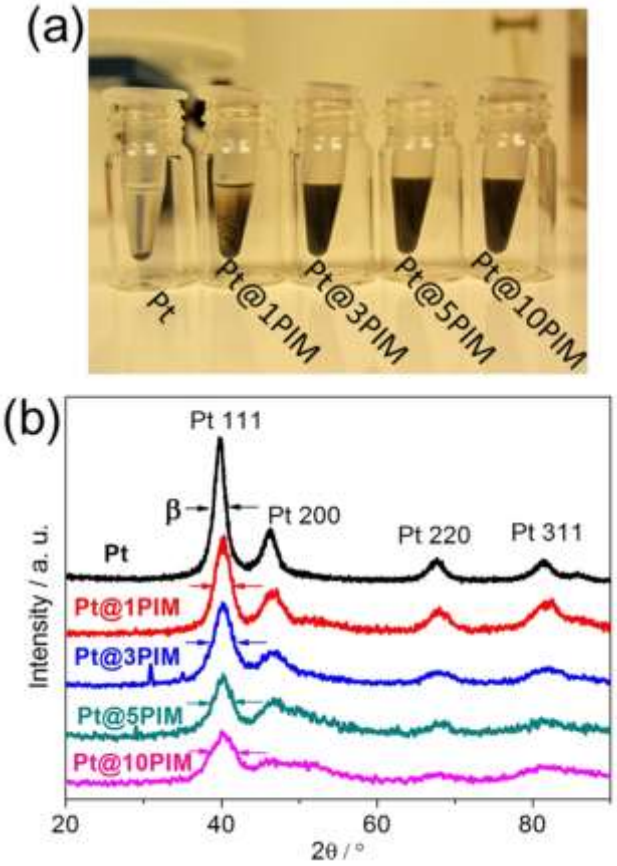

Figure 2. (a) Photographic image of Pt and Pt@PIM composites dispersed in ethanol after 12 h settling time. (b) XRD patterns of Pt and Pt@PIM composites. The 111 peak was used for estimating particle size from the peak width at half height β.

XPS data (Figure 3) clearly confirms the presence of nitrogen in the Pt@PIM materials due to the structural nitrogen in the polymer. When analysed more closely, a shoulder is seen for the N1s peak (compare peaks for pure PIM-EA-TB at 399 and 401 eV[24]).

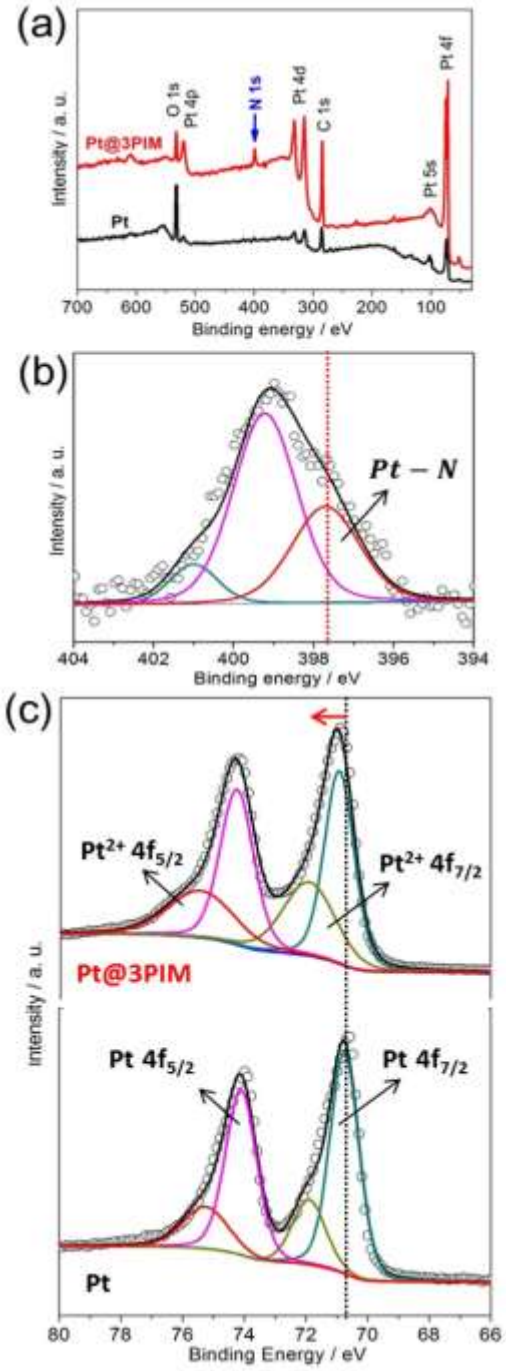

Figure 3. (a) XPS survey spectrum of Pt and Pt@3PIM. (b) XPS spectrum of N 1s for Pt@3PIM. (c) XPS spectra for the Pt(4f) bands for Pt@3PIM and Pt, respectively.

As shown in Figure 3b, the N (1s) line was deconvoluted into three superimposed peaks at 397.7, 399.2, and 401.0 eV. The peaks at 399.2 and 401.0 eV are consistent with those in PIM-EA-TB, which have been assigned to C-N nitrogen[25] and protonated nitrogen, respectively. The peak at 397.7 eV is likely to be associated with the presence of metal-nitrogen bond between the N-atom of PIM-EA-TB and the surface Pt-atoms of the Pt nanoparticles. Figure 3c shows two pairs of peaks for Pt 4f corresponding to metallic Pt and an oxide species. A slight shift to higher energy is found in the binding energies of the PIM-EA-TB stabilized Pt, but this may be due to charging in the polymer environment.

TEM images in Figure 4 directly confirm the presence of platinum nanoparticles. Figure 4a and 4b show the distributions and morphologies of Pt and Pt@3PIM samples produced under the same conditions. Crystalline Pt nanoparticles is evidenced in high resolution TEM images (see Figure 4d and 4f) by the lattice measurement. Without PIM-EA-TB the nanosized Pt particles are readily aggregated and grown into bigger particles (Figure 4d). In contrast, much smaller Pt nanoparticles with uniform size distribution can be seen for the PIM-EA-TB stabilized material shown in Figure 4e-h. Corresponding particle size distribution data are provided for each material calculated from more than 200 Pt nanoparticles. The Pt@3PIM sample shows a slightly narrower size distribution (3.1 ± 0.2 nm), which is approximately twice smaller than the nanoparticles in the Pt sample (6.1 ± 0.3 nm). Notably, the shape of the nanoparticles is spherical, rather than (truncated) cube or octahedron, which are often observed in strong ligand-facet interaction system, implying that the polymer does not have facet (for example {100} or {111}) preference. From TEM images it appears that samples are not necessarily homogenous with some darker regions being present at edges. Further characterization by electron energy loss spectroscopy (EELS) reveals a signal consistent with the presence of N (Figure 4c). A summary of materials and particle sizes is given in Table 1.

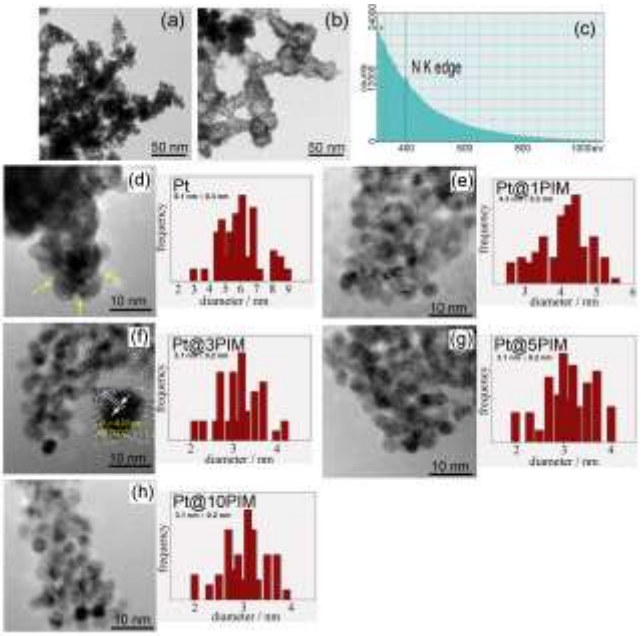

Figure 4. (a, b) TEM images and (c) EELS spectra taken in Pt@3PIM indicating the Pt-N interaction. (d-h) HRTEM images of Pt, Pt@1PIM, Pt@3PIM, Pt@5PIM, and Pt@10PIM.

Table 1. Summary of platinum particle size data from TEM measurements and estimated weight ratio.

Sample	**Weight ratio** /mg:mg [a]	/mg:mg [b]	**Particle diameter** /nm [c]
Pt	0.68 : 0	0.68 : 0	6.1
Pt@1PIM	0.68 : 0.1	0.68 : 0.011	4.3
Pt@3PIM	0.68 : 0.3	0.68 : 0.012	3.1
Pt@5PIM	0.68 : 0.5	0.68 : 0.016	3.1
Pt@10PIM	0.68 : 1.0	0.68 : 0.016	3.1

[a] weight of platinum : weight of PIM-EA-TB in 5 mL ethanol.

[b] weight of Pt : weight of C by elemental microanalysis.

[c] from TEM as average from >200 particles (see Figure 4).

When investigating Pt/C elemental analysis data (Table 1), it is apparent that most of the PIM-EA-TB polymer is lost in the washing step and only PIM-EA-TB firmly bound to Pt is captured in the composite. Saturation occurs for Pt@5PIM and Pt@10PIM, at which point additional polymer does not add to the carbon content. These data are consistent with the fact that at this point also stable colloids are formed and that the Pt nanoparticle diameter remains constant for Pt@5PIM and Pt@10PIM.

Electrochemical characterization of platinum nanoparticle networks in PIM-EA-TB. When studying the voltammetric signature of the platinum nanoparticles in aqueous 0.1 M $HClO_4$, typical responses associated with processes in the hydrogen region (-0.25~0.1 V), the double layer region (0.1~0.4 V), and the oxide region (0.4~0.95 V) are observed (see Figure 5a). From the area under the hydrogen region the electrochemically active surface area (ECA[26]) can be estimated. The ECA for the platinum was calculated from measuring the charge collected in the hydrogen adsorption/desorption region (see Q_H) and assuming a conversion constant of 210 μC cm^{-2}. Values are typically 10 to 20 m^2g^{-1}. Here, this ECA value reflects both (i) the total surface area of platinum present on the electrode surface and (ii) the electronic conduction through the Pt@xPIM composite material. Data in Figure 5b show an initial increase in surface area when adding the PIM-EA-TB stabilizing agent. This is consistent with the decreasing particle size and therefore increasing total surface area. However, at higher polymer content beyond Pt@3PIM the apparent surface area (ECA) decreases again. This is in spite of the platinum nanoparticle diameter remaining small (see Table 1). This observation can be rationalized here based on the loss of electronic conductivity (loss of conductivity at the percolation threshold or loss of conductivity due to too much rigid capping agent).

There are two possible reasons for the loss of electronic conductivity: (i) platinum particles are smaller in size so that the rate of tunneling of electrons across the rigid polymer backbone holding the platinum particles becomes insufficient (radius *r* is decreased) or (ii) the "occupancy" of platinum particles in nitrogen sites along the polymer backbone is decreased to the point that the inter-particle distance is too long for electron tunneling. Both scenarios could contribute to the observed behavior.

It may be possible to consider the case of Pt@3PIM consistent with not more than one "capping layer" inter-particle distance, as opposed to the Pt@5PIM and Pt@10PIM cases, where "saturation in capping" could lead to inter-platinum particle distances higher than the maximum tunnel distance. Conductivity in nanoparticle assemblies is strongly dependent on the inter-particle distance[27] and models based on percolation transport have been developed to explain conductivity quantitatively. An inter-particle tunnel distance of approximately 1 to 2 nm is often considered feasible,[28] but for longer distance tunneling the rate drops exponentially, which is likely to cause loss of electrical conductivity. For Pt@3PIM a limit seems to be reached with apparent loss in electrochemically active platinum surface area beyond this point.

In terms of future applications, Pt@3PIM offers a highly electrochemically active surface area (for example for electrocatalysis) and possibly a high sensitivity towards reversible swelling and deformation (for sensing in smart devices). Conducting nanoparticle networks may also be relevant in percolating networks with neuromorphic behavior[29] and in particular in stress and pressure sensors[30] or in gas sensors.[31]

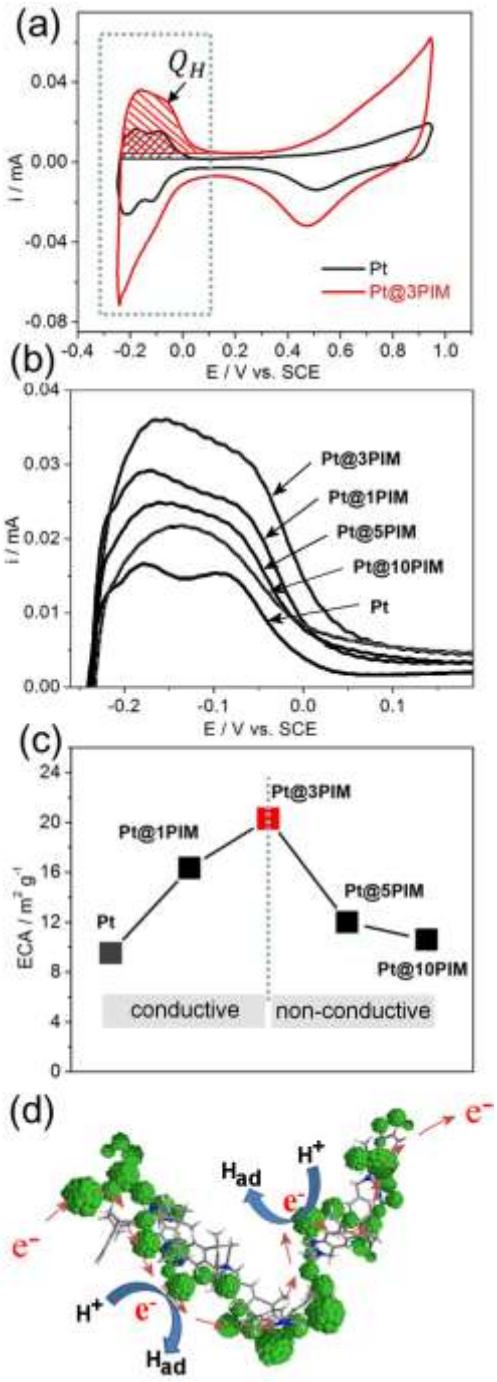

Figure 5. (a) Cyclic voltammograms (scan rate 0.05 Vs^{-1}) for Pt and Pt@3PIM immersed in 0.1 M $HClO_4$. (b) Hydrogen adsorption region within cyclic voltammograms for different samples. (c) Electrochemically active surface area (ECA) versus Pt@PIM sample. (d) Schematic mechanism of hydrogen adsorption/desorption in PIM-EA-TB stabilized Pt coupled to electrical conductivity.

Conclusion. It has been shown that PIM-EA-TB can be employed to grow and to stabilize platinum nanoparticles in ethanolic solution. The nanoparticles form with approximately 3 – 4 nm diameter (depending on platinum to polymer weight ratio) and the inter-particle distance is affected by the resulting platinum to PIM-EA-TB volume ratio and the extent of capping with rigid PIM-EA-TB. The inter-particle distance is likely to be an important parameter in providing electrical conductivity through the network, but further work will be required to determine and explore this parameter, for example also in conjunction with the molecular weight of the polymeric capping agent. In future, nanocomposite materials based on PIM-EA-TB with embedded nanoparticles could be of wider use. As a highly molecularly rigid structure PIM-EA-TB offers binding sites without blocking embedded metal nanoparticle surface sites, which could be of use in catalysis. Other types of metal or metal oxide nanostructures could be embedded into the PIM host for applications in a wider range of applications including sensing devices.

AUTHOR INFORMATION

Corresponding Author

Frank Marken, Department of Chemistry, University of Bath, Claverton Down, Bath BA2 7AY, UK, email f.marken@bath.ac.uk

ACKNOWLEDGMENT

D.H. thanks the Royal Society for a Newton International Fellowship. F.M. and N.B.M. thank the Leverhulme Foundation for financial support (RPG-2014-308: New Materials for Ionic Diodes and Ionic Photodiodes").

REFERENCES

(1) Na, K.; Zhang, Q.; Somorjai, G.A. Colloidal Metal Nanocatalysts: Synthesis, Characterization, and Catalytic Applications. *J. Cluster Sci.* **2014**, *25*, 83-114.
(2) Niu, Z.Q.; Li, Y.D. Removal and Utilization of Capping Agents in Nanocatalysis. *Chem. Mater.* **2014**, *26*, 72-83.
(3) Leong, G.J.; Schulze, M.C.; Strand, M.B.; Maloney, D.; Frisco, S.L.; Dinh, H.N.; Pivovar, B.; Richards, R.M. Shape-directed Platinum Nanoparticle Synthesis: Nanoscale Design of Novel Catalysts. *Appl. Organomet. Chem*. **2014**, *28*, 1-17.
(4) Guo, S.J.; Zhang, S.; Sun, S.H. Tuning Nanoparticle Catalysis for the Oxygen Reduction Reaction. *Angew. Chem., Int. Ed.* **2013**, *52*, 8526-8544.
(5) Dhakshinamoorthy, A.; Garcia, H. Catalysis by Metal Nanoparticles Embedded on Metal-organic Frameworks *Chem. Soc. Rev*. **2012**, *41*, 5262-5284.
(6) Budd, P.M.; Ghanem, B.S.; Makhseed, S.; McKeown, N.B.; Msayib, K.J.; Tattershall, C.E. Polymers of Intrinsic Microporosity (PIMs): Robust, Solution-processable, Organic Nanoporous Materials *Chem. Commun.* **2004**, 230-231.
(7) McKeown, N.B.; Budd, P.M. Polymers of Intrinsic Microporosity (PIMs): Organic Materials for Membrane Separations, Heterogeneous Catalysis and Hydrogen Storage *Chem. Soc. Rev*. **2006**, *35*, 675-683.
(8) Chen, X.Y.; Vinh-Thang, H.; Ramirez, A.A.; Rodrigue, D.; Kaliaguine, S. Membrane Gas Separation Technologies for Biogas Upgrading *RSC Adv.* **2015**, *5*, 24399-24448.
(9) Hart, K.E.; Colina, C.M. Ionomers of Intrinsic Microporosity: In Silico Development of Ionic-Functionalized Gas-Separation Membranes *Langmuir*, **2014**, *30*, 12039-12048.
(10) Carta, M.; Malpass-Evans, R.; Croad, M.; Rogan, Y.; Jansen, J.C.; Bernardo, P.; Bazzarelli, F.; McKeown, N.B. An Efficient Polymer Molecular Sieve for Membrane Gas Separations. *Science*, **2013**, *339*, 303-307.
(11) Wang, Y.; McKeown, N.B.; Msayib, K.J.; Turnbull, G.A.; Samuel, I.D.W. Laser Chemosensor with Rapid Responsivity and Inherent Memory Based on a Polymer of Intrinsic Microporosity. *Sensors*, **2011**, *11*, 2478-2487.
(12) Madrid, E.; Rong, Y.Y.; Carta, M.; McKeown, N.B.; Malpass-Evans, R.; Attard, G.A.; Clarke, T.J.; Taylor, S.H.; Long, Y.T.; Marken, F. Metastable Ionic Diodes Derived from an Amine-Based Polymer of Intrinsic Microporosity. *Angew. Chem., Int. Ed.* **2014**, *53*, 10751-10754.
(13) Rong, Y.Y.; Kolodziej, A.; Madrid, E.; Carta, M.; Malpass-Evans, R.; McKeown, N.B.; Marken, F. Polymers of Intrinsic Microporosity in Electrochemistry: Anion Uptake and Transport Effects in Thin Film Electrodes and in Free-standing Ionic Diode Membranes. *J. Electroanal. Chem*. **2015**, doi:10.1016/j.jelechem.2015.11.038.
(14) Madrid, E.; Cottis, P.; Rong, Y.Y.; Rogers, A.T.; Stone, J.M.; Malpass-Evans, R.; Carta, M.; McKeown, N.B.; Marken, F. Water Desalination Concept Using an Ionic Rectifier Based on a Polymer of Intrinsic Microporosity (PIM). *J. Mater. Chem. A* **2015**, *3*, 15849-15853.
(15) He, D.P.; Rong, Y.Y.; Carta, M.; Malpass-Evans, R.; McKeown, N.B.; Marken, F. Fuel Cell Anode Catalyst Performance can be Stabilized with a Molecularly Rigid Film of Polymers of Intrinsic Microporosity (PIM). *RSC Adv*., **2016**, *6*, 9315-9319.
(16) He, D.P.; Rong, Y.Y.; Kou, Z.K.; Mu, S.C.; Peng, T.; Malpass-Evans, R.; Carta, M.; McKeown, N.B.; Marken, F. Intrinsically Microporous Polymer Slows Down Fuel Cell Catalyst Corrosion. *Electrochem. Commun*. **2015**, *59*, 72-76.
(17) Rong, Y.Y.; Malpass-Evans, R.; Carta, M.; McKeown, N.B.; Attard, G.A.; Marken, F. High Density Heterogenisation of Molecular Electrocatalysts in a Rigid Intrinsically Microporous Polymer. *Electrochem. Commun*. **2014**, *46*, 26-29.
(18) Kolodziej, A.; Ahn, S.D.; Carta, M.; Malpass-Evans, R.; McKeown, N.B.; Chapman, R.S.L.; Bull, S.D.; Marken, F. Electrocatalytic Carbohydrate Oxidation with 4-Benzoyloxy-TEMPO Heterogenised in a Polymer of Intrinsic Microporosity. *Electrochim. Acta,* **2015**, *160*, 195-201.
(19) Althumayri, K.; Harrison, W.J.; Shin, Y.Y.; Gardiner, J.M.; Casiraghi, C.; Budd, P.M.; Bernardo, P.; Clarizia, G.; Jansen, J.C. The Influence of Few-layer Graphene on the

Gas Permeability of the High-free-volume Polymer PIM-1. *Philos. Trans. R. Soc., A* **2016**, *374*, 20150031.
(20) Hasell, T.; Wood, C.D.; Clowes, R.; Jones, J.T.A.; Khimyak, Y.Z.; Adams, D.J.; Cooper, A.I. Palladium Nanoparticle Incorporation in Conjugated Microporous Polymers by Supercritical Fluid Processing. *Chem. Mater.* **2010**, *22*, 557-564.
(21) Bronstein, L.M.; Goerigk, G.; Kostylev, M.; Pink, M.; Khotina, I.A.; Valetsky, P.M.; Matveeva, V.G.; Sulman, E.M.; Sulman, M.G.; Bykov, A.V.; Lakina, N.V.; Spontak, R.J. Structure and Catalytic Properties of Pt-modified Hyper-cross-linked Polystyrene Exhibiting Hierarchical Porosity. *J. Phys. Chem. B* **2004**, *108*, 18234-18242.
(22) Xia, F.J.; Pan, M.; Mu, S.C.; Malpass-Evans, R.; Carta, M.; McKeown, N.B.; Attard, G.A.; Brew, A.; Morgan, D.J.; Marken, F. Polymers of Intrinsic Microporosity in Electrocatalysis: Novel Pore Rigidity Effects and Lamella Palladium Growth. *Electrochim. Acta,* **2014**, *128*, 3-9.
(23) Holzwarth, U.; Gibson, N. The Scherrer Equation Versus the 'Debye-Scherrer Equation'. *Nat. Nanotechnol.* **2011**, *6*, 534-534.
(24) Rong, Y.Y.; He, D.P.; Sanchez-Fernandez, A.; Evans, C.; Edler, K.J.; Malpass-Evans, R.; Carta, M.; McKeown, N.B.; Clarke, T.J.; Taylor, S.H.; Wain, A.J.; Mitchels, J.M.; Marken F. Intrinsically Microporous Polymer Retains Porosity in Vacuum Thermolysis to Electroactive Heterocarbon. *Langmuir*, **2015**, *31*, 12300-12306.
(25) Moayeri, A.; Ajji, A. Fabrication of Polyaniline/poly(ethylene oxide)/Non-covalently Functionalized Graphene Nanofibers via Electrospinning. *Synth. Met.* **2015**, *200*, 7-15.
(26) Biegler, T.; Rand, D.A.J.; Woods, R. Limiting Oxygen Coverage on Platinized Platinum – Relevance to Determination of Real Platinum Area by Hydrogen Adsorption. *J. Electroanal. Chem*. **1971**, *29*, 269-274.
(27) Grisolia, J.; Decorde, N.; Gauvin, M.; Sangeetha, N.M.; Viallet, B.; Ressier, L. Electron Transport Within Transparent Assemblies of Tin-doped Indium Oxide Colloidal Nanocrystals. *Nanotechnology* **2015**, *26*, 335702.
(28) Zabet-Khosousi, A.; Dhirani, A.A. Charge Transport in Nanoparticle Assemblies. *Chem. Rev.* **2008**, *108*, 4072-4124.
(29) Fostner, S.; Brown, S.A. Neuromorphic Behavior in Percolating Nanoparticle Films. *Phys. Rev. E* **2015**, *92*, 052134.
(30) Farcau, C.; Sangeetha, N.M.; Moreira, H.; Viallet, B.; Grisolia, J.; Ciuculescu-Pradines, D.; Ressier, L. High-Sensitivity Strain Gauge Based on a Single Wire of Gold Nanoparticles Fabricated by Stop-and-Go Convective Self-Assembly. *ACS Nano* **2011**, *5*, 7137-7143.
(31) Krasteva, N.; Besnard, I.; Guse, B.; Bauer, R.E.; Müllen, K.; Yasuda, A.; Vossmeyer, T. Self-assembled Gold Nanoparticle/Dendrimer Composite Films for Vapor Sensing Applications. *Nano Lett*. **2002**, *2*, 551-555.